Aging-Sensitive Networks Within the Human Structural Connectome Are Implicated in Late-Life Cognitive Declines

Supplement 1

Table of Contents

1. Supplementary Methods

a. Methods and materials.

i. UK Biobank. A large-scale population epidemiology study, UK Biobank (UKB) involved the recruitment of approximately 500,000 individuals across Great Britain for medical, psychosocial, and biological data collection[1]. A subset of around 100,000 UKB participants were invited to complete brain MRI scanning (scanner details are provided in the next section); as of this writing, data collection is still in progress, but portions of the data have been made available. A total of 9,858 participants with compatible T1-weighted and diffusion tensor (dMRI) data were selected from the UK Biobank (exclusion criteria provided below). In the present study, 8,185 participants (4,315 female) who had usable MRI data were included, with an average age of 61.9 years (SD = 7.5, range = 44.64 – 78.17). All participants had usable volume data and reported their age at the time of scanning. 157 of the total 8,185 participants (< 2%) met for potentially confounding dementias and neurological syndromes (e.g., multiple sclerosis, stroke), though excluding these participants from the sample did not change primary outcome measures ($r_{\text{age correlations (before and after exclusion)}} > 0.999$, mean absolute difference = 0.001 for both edges and nodes). As such, we retain the full sample for our analyses. Despite previous research that has demonstrated neuroanatomical sex differences in men and women[2,3], we found largely similar patterns of connectome aging across men and women ($r_{\text{edge-age correlations}} = 0.892$; $r_{\text{node-age correlations}} = 0.974$, all p's < 0.0005). We did not further correct for biological sex. All the data from the present study come from the UK Biobank recruitment center in Manchester, UK. UKB received ethical approval from the Research Ethics Committee (reference 11/NW/0382). All participants provided informed consent to participate.

ii. Lothian Birth Cohort 1936. In 1947, almost all children attending schools in Scotland and born in 1936 completed an intelligence test as part of the Scottish Mental Survey 1947[4]. 1,091 of these individuals living mostly in the Edinburgh and Lothians area of Scotland were contacted and returned for re-testing at an average age of 69.5 years, becoming the Lothian Birth Cohort 1936 (LBC1936)[5,6], a longitudinal study of aging. As part of the second wave of testing, at age 72.8 years (SD = 0.70), 731 LBC1936 members underwent brain MRI scanning, of whom 528 (246 female) had reliable brain and cognitive data for the cognitive prediction analysis. Only age 11 IQ data, and data from this second wave of test (first wave of brain MRI) are included in the present study.

iii. UKB MRI. MRI data for all participants was collected on the same 3T Siemens Skyra MRI scanner (see Miller et al.[7] & Alfaro-Almagro et al.[8] for full details). A total of 9,858 participants with compatible T1-weighted data were selected from the UK Biobank. T1-weighted volumes were acquired in the sagittal plane using a 3D MP-RAGE sequence and preprocessed and analyzed using FSL tools (http://www.fmrib.ox.ac.uk/fsl) by the UKB brain imaging team. A full overview of the preprocessing and analysis pipeline is available at https://biobank.ctsu.ox.ac.uk/crystal/crystal/docs/brain_mri.pdf. Upon acquiring the raw data from UKB, FoV-reduced T1-weighted volumes were used to reconstruct and segment the cortical mantle using default parameters in FreeSurfer v5.3[9] (http://surfer.nmr.mgh.harvard.edu/) based on the Desikan-Killiany atlas[10]. Automated anatomical segmentation of subcortical structures (accumbens area, amygdala, caudate, hippocampus, pallidum, putamen, thalamus, ventral diencephalon, and brainstem) was also conducted in FreeSurfer using default settings and atlas[11]. Each output underwent visual assessment and participants with substantial motion artifact or major errors in skull stripping, tissue segmentation, or cortical parcellation were excluded. 8,185

participants remained after 842 were excluded due to incomplete FreeSurfer output or failure at QC.

iv. LBC1936 MRI. MRI data for all participants was collected on the same GE Signa Horizon HDx 1.5T clinical scanner (General Electric, Milwaukee, WI) equipped with a self-shielding gradient set (33 mT/m maximum gradient strength) and manufacturer supplied eight-channel phased-array head coil (see Wardlaw et al.[12] for full details). High-resolution T1-weighted volumes were acquired in the coronal plane using a 3D fast-spoiled gradient echo (FSPGR) and subsequently processed in FreeSurfer v5.1. As with the UK Biobank data, reconstruction and segmentation were based on the Desikan-Killiany atlas[10,11]. Segmentation and parcellation errors were corrected manually after visual inspection of each image.

v. Tractography. Probabilistic tractography pipelines were identical across both datasets, though acquisition procedures differed slightly. For UKB, dMRI acquisitions are publicly available from the UKB website in the form of a Protocol (http://biobank.ctsu.ox.ac.uk/crystal/refer.cgi?id=2367), Brain Imaging Documentation (and in Miller et al.[7])). The dMRI data were acquired using a spin-echo echo-planar imaging sequence (50 b = 1000 s/mm^2, 50 b = 2000 s/mm^2 and 10 b = 0 s/mm^2) resulting in 100 distinct diffusion-encoding directions. The field of view was 104 × 104 mm with imaging matrix 52 × 52 and 72 slices with slice thickness of 2 mm resulting in 2 × 2 × 2 mm voxels. 831 participants were excluded due to missing dMRI data or processing failure. For LBC1936, dMRI data was acquired from both T2-weighted and sets of diffusion-weighted (b = 1000 s/mm^2) axial single-shot spin-echo echo-planar (EP) volumes acquired with diffusion gradients applied in 64 noncollinear directions[12]. Both datasets were corrected for head motion and eddy currents, and processed using BEDPOSTx, with within-voxel modeling of multi-fibre tract orientation structure. BEDPOSTx processing was carried out by the UKB team prior to receiving the data. Upon acquiring the dMRI data, probabilistic tractography with crossing fiber modeling was carried out using PROBTRACKx[13]. Streamlines were seeded from all white matter voxels using 100 Markov Chain Monte Carlo iterations with a fixed step size of 0.5 mm between successive points.

vi. Statistical software. All analyses were run in R[14]. Graphics were created using the *ggplot2* package[15]. Anatomical network plots were created using BrainNet Viewer[16]. Factor modeling and structural regression models were estimated using the *lavaan* package[17]. LASSO model fitting and associated cross-validation was conducted within the *cv.glmnet* package[18], with wrapper functions from the *caret* package[19] in R. For graph-theory analyses, we used the *igraph*[20] package in R to compute network parameters.

b. Sensitivity analyses. To probe the uniqueness of signatures of whole-brain and network-specific connectome integrity in predicting cognitive function, we ran a series of sensitivity analyses.

i. Thresholding analyses. We probed whether associations between indices of connectome integrity and cognitive function were likely to be inflated by potentially spurious connections arising from the use of unthresholded data. In UKB, we re-estimated each connectome using a consistency-based thresholding approach[21], wherein connections are retained only if they have sufficiently low inter-subject variability in their weight and if their weight is plausibly strong for its length, which has been suggested as a method for removing connections that are most likely to be spurious. We correlated the age correlations and the PC loadings estimated in the unthresholded connectomes, either when the thresholded edges were set to 0, or when they were deleted entirely (1,071 edges retained).

ii. Permuted composites. We were interested in assessing whether the observed association between indices of connectome integrity and cognitive function were superior to those that would have been obtained had the weights used to create the indices been shuffled. We compared the observed associations between composite scores and all domains of cognitive function to associations with composite scores weighted by randomly-shuffled age correlations or PC loadings in the whole-brain. We shuffled weights for both edges and nodes in UKB (k = 1000 for each) by sampling with replacement from the observed age correlations or PC loadings (see Fig. 3). We then weighted and summed the LBC1936 connectomes by the shuffled weights, resulting in four random composite scores (edges and nodes weighted by either shuffled age correlations or shuffled PC loadings) for each participant. We calculated the association between processing speed, visuospatial ability, and memory and each of the 1000 permuted composites to arrive at an empirical null distribution. Observed associations were determined to be significant if they were smaller than the bottom 2.5%-ile or larger than the top 97.5%-ile of the empirical null distribution.

c. Regularized LASSO regression models. We first trained models to predict age in UK Biobank, and used the resulting predictive model to compute indices of connectome age in LBC1936, which we used to predict cognitive function.

i. Age prediction in UK Biobank. We fitted LASSO models predicting chronological age using connectome elements, as well as dummy variables representing the presence or absence of an element, in 80% of the UKB sample (~6,500 participants), with 10-fold cross-validation to select the optimal penalization parameter (λ) that provided the lowest prediction error. 10-fold cross-validation has been heralded as the gold-standard for obtaining accurate estimates from predictive models[22]. We then used the obtained coefficients to produce a score on *connectome age* in the 20% UKB holdout sample (~1,600 participants), which we used to predict chronological age. This process was repeated 100 times – reported coefficients were averaged across each of the 100 runs. For the whole-brain connectome, and for each network-of-interest (NOI), we ran analyses separately for edges and nodes, with all edges and nodes together, and with a novel topologically-constrained weighting scheme that takes into account the interactive effects of edges and nodes.

This procedure was run for each NOI, separately for the network's edges, nodes, and then with multiple weighting schemes reflecting the joint contribution edges and nodes together (see below for description). For edges, we included both the FA-weighting of each edge, as well as a binary dummy variable indicating whether or not the edge was present in a given participant.

Each iteration split a different random shuffle of the full dataset into training and testing samples. The results reported below for the variance explained in age by each network are the average R^2 values from this resampling procedure, and the standard error for each R^2 is the standard deviation of the values across all 100 iterations. We also report the R^2 adjusted by the size of the network by dividing by the number of elements in the included predictor set.

ii. Cognitive function prediction in LBC1936. For the final predictive analysis, we employed a similar pipeline to train for predicting cognitive function in LBC1936 from connectome elements, using LASSO models trained in UKB. We first fitted LASSO models predicting chronological age using connectome elements in UKB participants, with 10-fold cross-validation to select the optimal penalization parameter (λ). We then used the obtained coefficients to produce a score on *connectome age* in the narrow-aged LBC1936 sample, which we used to predict processing speed and visuospatial ability. Note that, because participants were virtually

identical in their age in LBC1936, any differences in their *connectome age* could not be attributable to actual differences in chronological ages.

iii. Alternative weighting schemes. To investigate whether edges and nodes, when considered jointly, were more strongly predictive of connectome or cognitive aging, we ran the LASSO-regression prediction analyses using elements from three joint-element weighting schemes: node + edge, node*edge, node*edge + node.

Node + edge. First, we sought to examine the contribution of nodes and edges considered additively. Under this weighting scheme, we included the raw elements from the structural connectome: node volumes (k = 85) and FA-weighted edges (k = 3,570). This weighting scheme thus allows us to prune our estimates of potentially redundant information provided *across* nodes and edges.

Node*edge. Next, we sought to examine the holistic interaction of nodes and edges as tripartite systems. That is, we were interested not only in how nodes and edges collectively contributed to connectome and cognitive aging, but how their interactions predicted these outcomes. The steps of this weighting scheme, with accompanying mathematical representations, are detailed below. To summarize, we began by creating a vector of the square root of the 85 node volumes for each participant in UKB. We then multiplied this vector by its transpose to create an 85x85 matrix of pairwise node weights in each participant. The off-diagonal elements in this matrix therefore encapsulate information about node integrity for pairwise combinations of nodes. Finally, we element-wise multiplied the pairwise node-weighted matrices by the edge-weighted (i.e., fractional anisotropy) matrices to create an 85x85 node*edge-weighted matrix in each participant. Elements in the resulting matrix are thus reflective of the strength of the connection between two nodes, as well as the structural integrity of these nodes. Our focus was on multiplicative, rather than additive, interactions between edges and nodes as we were interested in the holistic integrity of each pair of nodes and the connections between them, rather than merely the sum of their constituent parts. For example, if Node A has a robust volume and is strongly connected to Node B, but Node B is highly atrophied, then a coefficient measuring the systemic integrity of this neural pathway should adequately reflect the depreciable contribution of Node B to the system. That is, small values within a tripartite system should nullify larger values as we are interested in the unified structure of these systems. Thus, these matrices were used to estimate a network wherein edges represent not just white matter connections between regions, but the multiplicative effect of (sub)cortical volume by white matter connection strength.

Step 1: Create a vector of the square root of each node volume ($k = 85$) for each participant.

$$V = \begin{bmatrix} \sqrt{\text{vol}_1} \\ \sqrt{\text{vol}_2} \\ \vdots \\ \sqrt{\text{vol}_{85}} \end{bmatrix}$$

Step 2: Multiply the vector of node volumes by its transpose to create an 85x85 matrix, where cells represent the product of pairwise volumes.

$$\text{Node-weighted Network} = VV^T = \begin{bmatrix} \sqrt{\text{vol}_1} \\ \sqrt{\text{vol}_2} \\ \vdots \\ \sqrt{\text{vol}_{85}} \end{bmatrix} \begin{bmatrix} \sqrt{\text{vol}_1} & \sqrt{\text{vol}_2} & \dots & \sqrt{\text{vol}_{85}} \end{bmatrix}$$

$$= \begin{pmatrix} \text{vol}_1 & & & & \\ \sqrt{\text{vol}_1} \cdot \sqrt{\text{vol}_2} & \text{vol}_2 & & & \\ \sqrt{\text{vol}_1} \cdot \sqrt{\text{vol}_3} & \sqrt{\text{vol}_2} \cdot \sqrt{\text{vol}_3} & \text{vol}_3 & & \\ \vdots & \vdots & \vdots & \ddots & \\ \sqrt{\text{vol}_1} \cdot \sqrt{\text{vol}_{85}} & \sqrt{\text{vol}_2} \cdot \sqrt{\text{vol}_{85}} & \sqrt{\text{vol}_3} \cdot \sqrt{\text{vol}_{85}} & \cdots & \text{vol}_{85} \end{pmatrix}$$

Step 3: Assemble the 85x85 edge-weighted matrix, where cells represent the microstructural connections between pairwise nodes.

$$\text{Edge-weighted Network} = F = \begin{pmatrix} 1 & & & & \\ \text{FA}_{1,2} & 1 & & & \\ \text{FA}_{1,3} & \text{FA}_{2,3} & 1 & & \\ \vdots & \vdots & \vdots & \ddots & \\ \text{FA}_{1,85} & \text{FA}_{2,85} & \text{FA}_{3,85} & \cdots & 1 \end{pmatrix}$$

Step 4: Element-wise multiply the node-weighted matrix by the edge-weighted matrix to create an edge & node weighted matrix, where cells represent the multiplicative interaction between pairwise node volumes and the connection strength between those nodes.

$$\text{Edge \& Node Weighted Network} = F \circ VV^T = \begin{pmatrix} 1 \cdot \text{vol}_1 & & & & \\ \text{FA}_{1,2} \cdot \sqrt{\text{vol}_1} \cdot \sqrt{\text{vol}_2} & 1 \cdot \text{vol}_2 & & & \\ \text{FA}_{1,3} \cdot \sqrt{\text{vol}_1} \cdot \sqrt{\text{vol}_3} & \text{FA}_{2,3} \cdot \sqrt{\text{vol}_2} \cdot \sqrt{\text{vol}_3} & 1 \cdot \text{vol}_3 & & \\ \vdots & \vdots & \vdots & \ddots & \\ \text{FA}_{1,85} \cdot \sqrt{\text{vol}_1} \cdot \sqrt{\text{vol}_{85}} & \text{FA}_{2,85} \cdot \sqrt{\text{vol}_2} \cdot \sqrt{\text{vol}_{85}} & \text{FA}_{3,85} \cdot \sqrt{\text{vol}_3} \cdot \sqrt{\text{vol}_{85}} & \cdots & 1 \cdot \text{vol}_{85} \end{pmatrix}$$

Node*edge + node. Lastly, we were interested in assessing whether the node*edge weighting scheme contributed more predictive power when nodes were included. Theoretically, if all useful information provided by nodes was captured in the node*edge weights, then the contribution of node volumes would have been redundant and dropped during the regularization process. Like the node + edge weighting scheme, this weighting scheme includes the 85 node volumes and the 3,570 node*edge weights.

2. Supplementary Results

a. Sensitivity analyses.

i. Thresholding analyses. Both unthresholded age correlations and loadings showed very strong linear relationships with thresholded versions of these metrics (*r*s > 0.999; Fig. S1). When thresholded edges were fixed to 0, rather than discarded, unthresholded age correlations correlated with thresholded age correlations at $r = 0.790$, and unthresholded loadings correlated with thresholded loadings at $r = 0.899$. These results indicate that potentially spurious connections were unlikely to substantially bias the results reported in this article. Despite this substantial overlap, previous work in this dataset has found that thresholding significantly improves average fractional anisotropy associations with age relative to unthresholded data[21].

ii. Permuted composites. Results of the permutation tests are reported in Table S9 and Fig. S10. For edges, the associations between composite scores and processing speed and visuospatial ability were statistically significant relative to the permuted distribution (empirical *p*'s < 0.01). Associations between observed edge-based composites and memory were statistically significant relative to the permuted distribution at empirical *p*'s < 0.05. In contrast, all associations for node composite scores fell within the middle of the permuted distribution for associations with both processing speed and visuospatial ability (empirical *p*'s > 0.09).

b. Intercorrelations between network-specific PC-weighted composite scores. We examined associations between composite indices of integrity within each NOI. Specifically, we computed intercorrelations amongst the network-specific PC-weighted composite scores for both edges and nodes to assess whether the general dimensions of network-specific integrity reflected an even broader dimension of whole-brain integrity (Fig. 2D; Fig. S3). Within edge-based composites, the average intercorrelation was 0.549 (interquartile range = 0.396 to 0.751; Table S7), with the first PC accounting for 62.2% of the variation in edge-based composite score covariance. Within node-based composites, the average intercorrelation was 0.827 (interquartile range = 0.749 to 0.892; Table S7), with the first PC accounting for 84.7% of variation in node-based composite score covariance. Edge-based composite scores and node-based composite scores were relatively uncorrelated within networks (see Table S8). Thus, after aggregating individual elements together according to NOIs, we observed strong correlations across the edge and node integrities of the different subnetworks. This is likely to be attributable both to the aggregation signal across elements within NOIs, that is itself correlated across NOIs, and to the overlap of elements within NOIs.

c. Network-specific aging occurs along general dimensions of variation in edge and node integrity. Edges from several NOIs showed patterns consistent with the whole brain (Figs. S5 & S6). In the Central Executive, Cingulo-Opercular, Default Mode, Multiple Demand, PFIT, and Temporo-Amygdala-Orbitofrontal networks, edges with higher PC loadings tended to have stronger negative correlations with age (*r*s = -0.820 to -0.508). The Sensorimotor network was the only NOI to show a moderately strong positive association between PC loadings and age correlations ($r = 0.382$), suggesting that edges that are more central to the integrity of this network tend to be less susceptible to ageing-related degradation.

On average, within-NOI node results were similar to within-NOI edge results. Across several NOIs, there was a negative relationship observed between age correlations and PC loadings (*r*s = -0.903 to -0.313 in the Cingulo-Opercular, Default Mode, Hippocampal-Diencephalic,

Multiple Demand, PFIT, Salience, and Temporo-Amygdala-Orbitofrontal networks). It is important to note that in certain networks (e.g., the Central Executive network), all nodes had consistently strong PC loadings *and* age correlations (age *r*s < -0.165; PC loadings (λs > 0.70)), resulting in a weak association between the PC loadings and age correlations (r = -0.076).

d. Associations between topological centrality, PC loadings, and age correlations in UKB. To quantify the weighted connectedness of each node in the whole-brain network, we calculated its topological *strength* (i.e., sum of adjacent edge weights), which we then averaged across participants. To quantify the weighted connectedness of each edge in the whole-brain network, we calculated the average topological strength (i.e., average sum of adjacent edge weights) of the two nodes connected by that edge, which we then averaged across participants. We found that the topological strengths of both edges and nodes were strongly correlated with loadings on their respective PCs (r_{edges} = 0.655; r_{nodes} = 0.583; all p's < 0.0005; see Fig. S7), suggesting that more topologically central elements within the connectome are more broadly representative of individual differences in the integrity of those elements. Importantly, this association is not due to a mathematical dependency between topological strength and principal component loadings, as topological strength is based on the absolute value of the edge weights whereas PC loadings are based on their covariation. The topological strength of an element was only modestly associated with its age correlation (r_{edges} = -0.202, p < 0.0005; r_{nodes} = -0.211, p = 0.053; Fig. S8). Topological centrality is therefore insufficient to explain the observed associations between PC loadings and age correlations. In other words, connectome aging occurs along general dimensions of *variation* in edge and node integrity, but occurs only modestly, and proportionally, to the amount of topological connectedness of structural connectome elements.

e. Results of regularized LASSO regression models.

i. Prediction of age in the UKB hold-out sample. Figure S12 displays the raw and adjusted R^2 values for each network for the LASSO regression prediction of age in the UK Biobank hold-out sample. Across the whole brain and all networks, edges alone explained greater variance in age than nodes alone (R^2 = 0.174 to 0.546 in edges; 0.073 to 0.358 in nodes). The model based on edges alone had good prediction accuracy in a holdout subsample (RMSE = 5.03 years). The model based on nodes alone showed slightly worse prediction accuracy than the model based on edges alone (RMSE = 5.97 years. Edges from the PFIT and Temporo-Amygdala-Orbitofrontal networks accounted for the greatest variation in age (R^2 = 0.385, 95% CI = [0.354, 0.416]; R^2 = 0.318, 95% CI = [0.288, 0.347], respectively).

Adjusted estimates indicated that nodes explained substantially greater variance in age than edges (R^2 = 0.0040 to 0.0188 for nodes; R^2 = 0.0002 to 0.0062 for edges). Similar to the weighted-composite analyses, edges from the whole brain, PFIT and Temporo-Amygdala-Orbitofrontal networks explained substantially less variance in age than all other networks (R^2 = 0.0001 to 0.0006, 95% CIs = [0.0001, 0.0007]). The same pattern of results was found for nodes (R^2 = 0.0040 to 0.0055, 95% CIs = [0.0032, 0.0063]), collectively suggesting that the age-relevant information contained in these networks is a product of their overall size, rather than reflecting a particular concentration of age-susceptible elements. Overall, when adjusted for the number of elements in the network, nodes provided more substantial prediction of age.

Removing potentially spurious edges with consistency-based thresholding prior to conducting the LASSO analyses slightly depreciated predictions relative to unthresholded data (mean ratio of unthresholded R^2 to thresholded R^2 across NOIs = 0.763). The Salience network

displayed a substantial difference in age prediction when using thresholded edges (mean ratio of unthresholded R^2 to thresholded R^2 = 0.314). To note, the correlation between mean edge weight and age within the Salience network remained positive, even after removing thresholded edges (r = 0.094, $p < 0.0005$), indicating that the reported positive age trends in the Salience network are not simply an artifact of potentially spurious connections. Looking across all edges, however, prediction with thresholded data was nearly identical to prediction with unthresholded data, suggesting the utility of LASSO in zero-weighting uninformative edges (whole-brain R^2 = 0.540; ratio of unthresholded R^2 to thresholded R^2 in whole brain = 0.988).

ii. Prediction of cognitive function in LBC1936. Figure S14 displays the raw and adjusted prediction results for processing speed and visuospatial ability. We confine our prediction to processing speed and visuospatial ability, as memory was not associated with connectome integrity above and beyond age-11 IQ (Table 2, main text). In contrast to the age-prediction results, nodes were substantially more predictive of both domains of cognitive function than were edges (whole-brain nodes: $r_{\text{processing speed}}$ = -0.198; 95% CI = [-0.288, -0.108]; $r_{\text{visuospatial ability}}$ = -0.165; 95% CI = [-0.259, -0.071]; whole-brain edges: $r_{\text{processing speed}}$ = 0.069; 95% CI = [-0.025, 0.163]; $r_{\text{visuospatial ability}}$ = 0.052; 95% CI = [-0.046, 0.150]). For processing speed, node-based associations were of comparable magnitude across NOIs (rs = -0.256 to -0.154, except in the Salience network, where r = -0.027). For visuospatial ability, nodes demonstrated somewhat more varied associations, with the Central Executive, Default Mode, and PFIT networks all displaying rs stronger than -0.300. Such correlation magnitudes are comparable to the associations using the weighted composite scores (Fig. 4), demonstrating that prediction of cognitive function using grey-matter elements is retained in the context of a regularization approach that favors sparsity of the predictor set. Edge-based connectome age, by contrast, displayed relatively weak associations with both processing speed and visuospatial ability across NOIs (rs = -0.099 – 0.094; -0.103 to 0.034, respectively). These associations were somewhat lower than the weighted composite scores, indicating that the statistical-learning algorithm did not retain the same predictive ability for cognitive function.

Consistent with the composite analyses, node-based connectome age from the Central Executive network retained the strongest adjusted correlations with both processing speed and visuospatial ability of any network (r_{adj} for processing speed = -0.0271, 95% CI = [-0.0384, -0.0159]); r_{adj} for visuospatial ability = -0.0416, 95% CI = [-0.0527, -0.0306]). Across both processing speed and visuospatial ability, the Multiple Demand, Sensorimotor, and Default Mode networks demonstrated the strongest adjusted associations after the Central Executive network (r_{adj} range = -0.0179 to -0.0160 for processing speed; r_{adj} range = -0.0238 to -0.0194 for visuospatial ability).

f. Age and cognitive prediction using novel weighting schemes.

i. Age prediction. The additive contribution of edges and nodes from across the whole brain explained the greatest variance in age (R^2 = 0.584, 95% CI = [0.560, 0.607]). This pattern was consistent across almost all NOIs (R^2 = 0.216 to 0.423), indicating the collective importance of all elements to brain aging (see Fig. S13). The novel node*edge and node*edge + node weighting schemes demonstrated approximately similar predictive power to the nodes + edges scheme across all NOIs and the whole brain (R^2 = 0.191 to 0.548 for node*edge; R^2 = 0.218 to 0.556 for node*edge + node), outperforming nodes alone in all NOIs, and displaying comparable associations to edges alone in all NOIs.

ii. Cognitive prediction. The magnitude of associations between weighting schemes and cognitive function varied by both network and cognitive domain (see Fig. S15). As with the age

prediction results, the three joint weighting schemes performed relatively consistently across both domains of cognitive function (*r*s = -0.162 to 0.116 for nodes + edges; *r*s = -0.239 to 0.081 for nodes*edges; *r*s = -0.155 to 0.114 for nodes*edges + nodes). Across all almost all networks, nodes alone outperformed all other weighting schemes (*r*s = -0.333 to -0.027). Thus, in the context of a LASSO approach that removes redundant predictors of the first-stage outcome (age), information relevant to cognitive function appears to be diluted by the inclusion of edges in addition to nodes.

3. Supplementary Figures

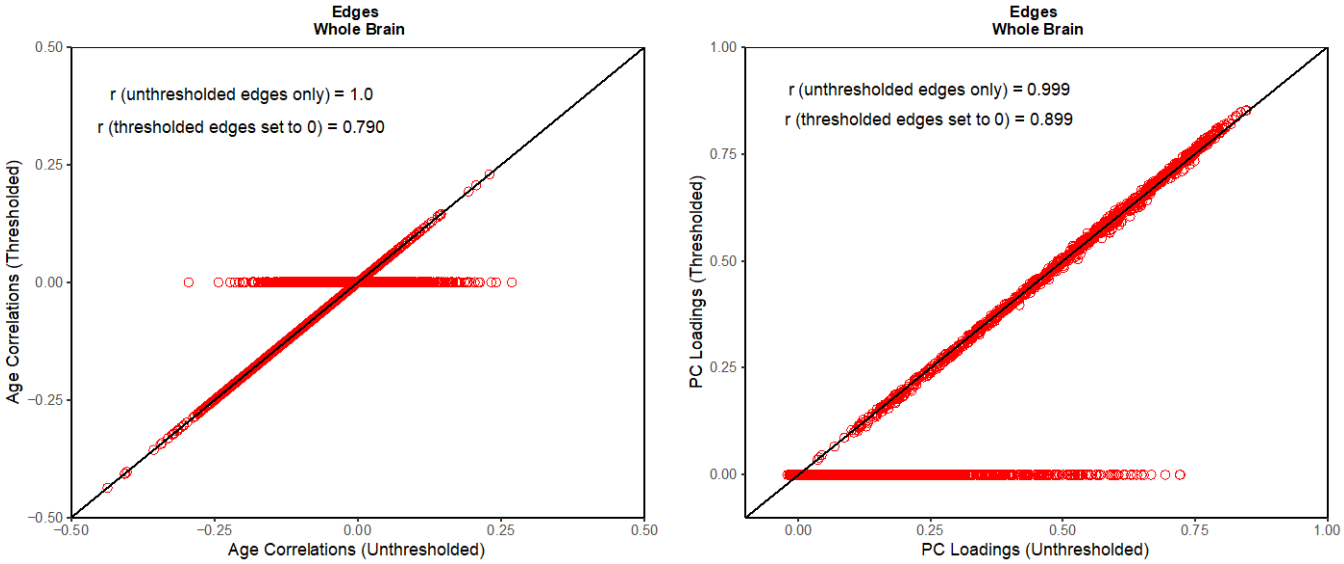

Figure S1. **Scatterplots of thresholded versus unthresholded edges.** Whole-brain associations between unthresholded and thresholded versions of age correlations and PC loadings. Thresholding was determined by a consistency based-approach[21]. We report correlations both including and excluding thresholded edges (N = 2,499). Regression line represents a slope of 1 (i.e., X = Y).

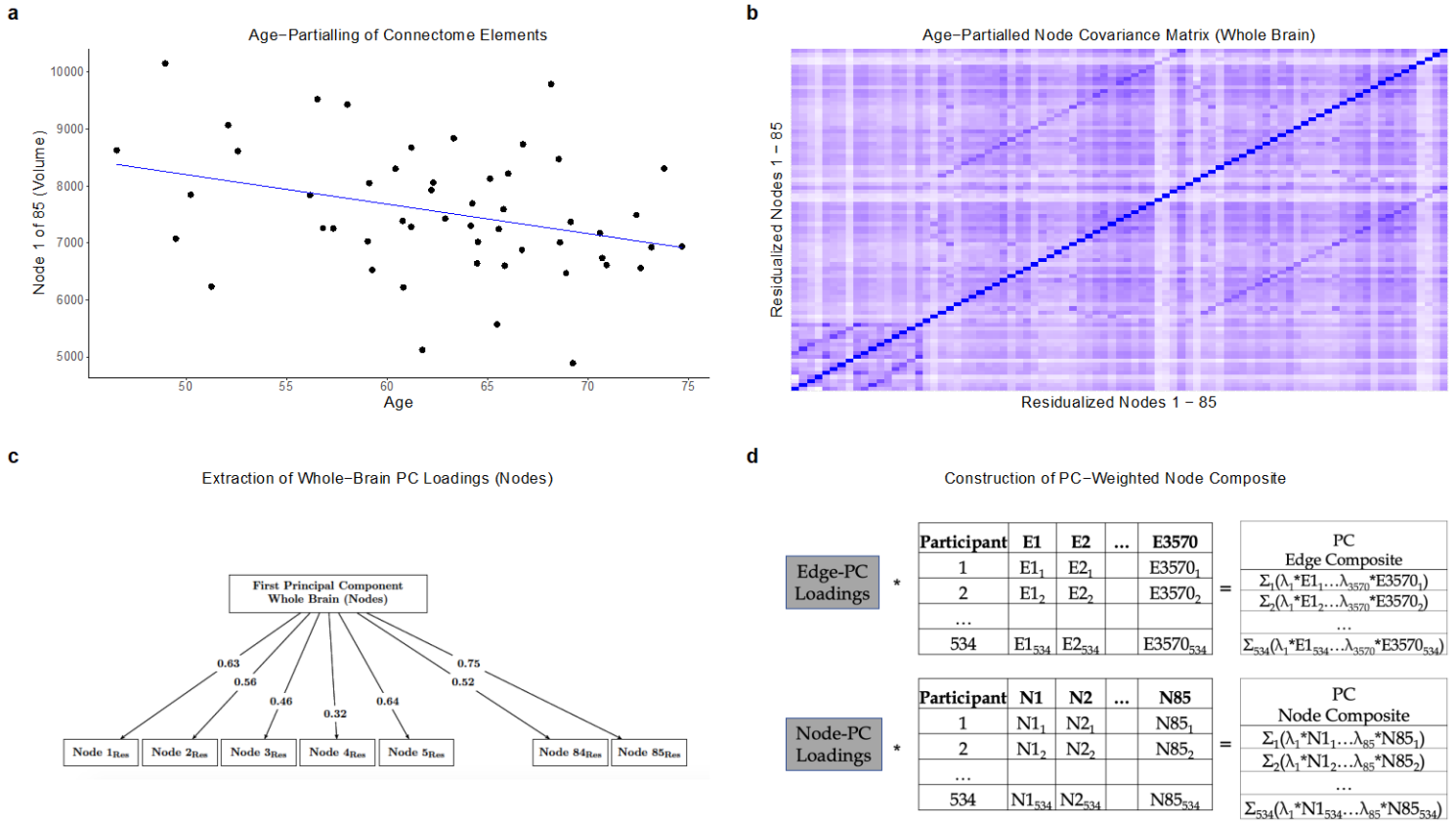

Figure S2. **Analytic pipeline for obtaining general dimensions of element integrity. a)** Scatterplot between Node 1 volume and age in UKB. Red line segments represent each participant's residual Node 1 (left Thalamus) integrity after removing age-related variance. This procedure was conducted for every element. Only 50 of the total 8,185 UKB participants are displayed for the sake of visual presentation. **b)** Whole-brain covariance matrix for residualized node integrities. Matrices were subjected to an Eigen decomposition to obtain general dimensions of age-partialled edge and node covariation (i.e., PCs). This procedure was conducted for the 3,567 edges that varied (of 3,570 total) and 85 nodes across the whole brain, as well as within each network, using only the elements contained within each specific NOI. **c)** Extraction of each residualized node's loading on the first whole-brain PC. We estimated loadings on the first PC derived from the edge and node covariance matrices. **d)** The UKB-derived PC loadings were then used to weight the raw edge and node integrities in LBC1936, such that each LBC1936 participant's element integrities were multiplied by their respective PC loading and then summed to create a single numerical index of connectome integrity. This procedure was conducted in the whole brain (i.e., using the whole-brain PC loadings) and within each network (i.e., using the network-specific PC loadings and summing only those elements contained within that network), separately for edges and nodes. The same analysis was conducted using the UKB-derived age correlations, instead of PC loadings, as weights.

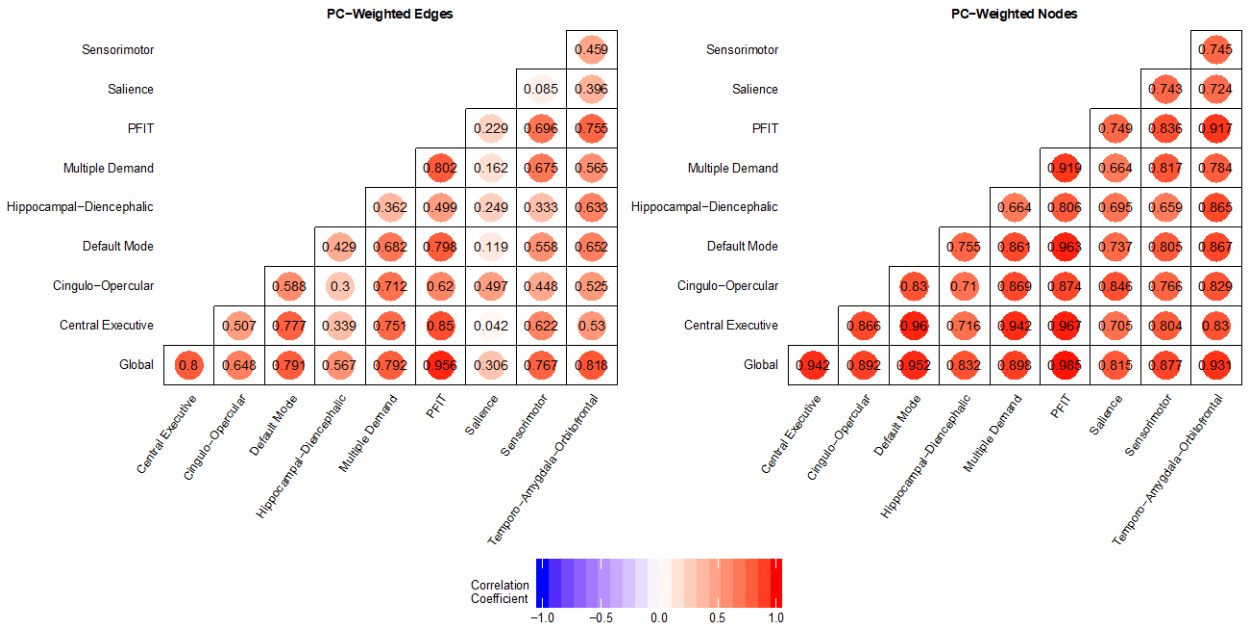

Figure S3. **Heatmaps of intercorrelations amongst PC-weighted composite scores.** Heatmaps of the correlations between PC-weighted composite scores created in each of the nine prespecified brain networks and whole brain. Correlations were estimated in edges and nodes separately. The interquartile range for correlations is presented in Table S7. Average correlations between edge- and node-based composites in each network are presented in Table S8.

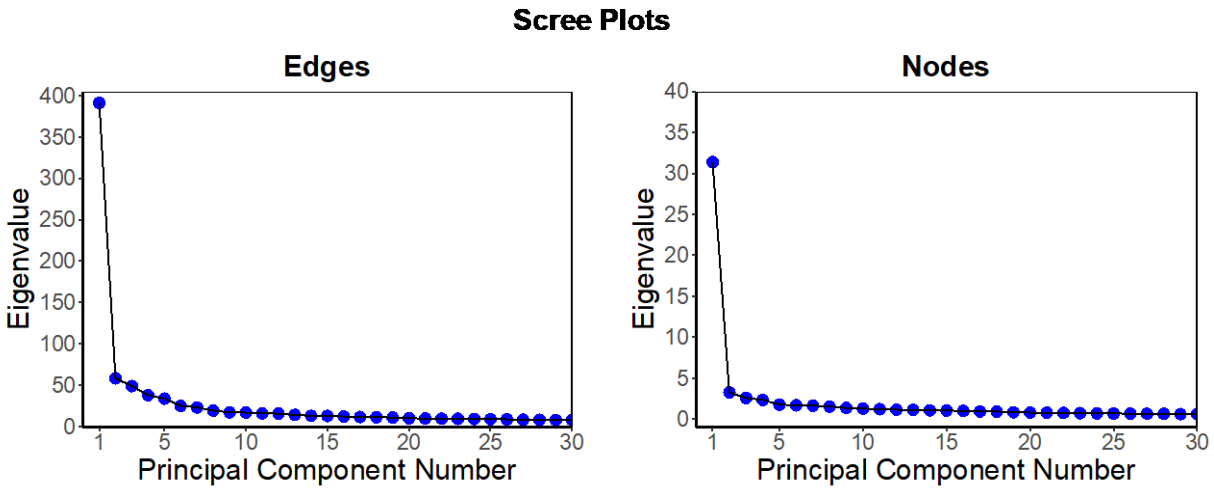

Figure S4. **Scree plots for whole-brain edge and node Eigen decompositions.** Scree plots reflecting the total variance explained by each principal component for edges and nodes separately. Principal components were estimated from covariance matrices of edges and nodes in UKB participants (N = 8,185). Loadings on the first principal component were used to investigate individual differences in global connectome integrity and were used to create weighted connectome integrity composite scores in LBC1936.

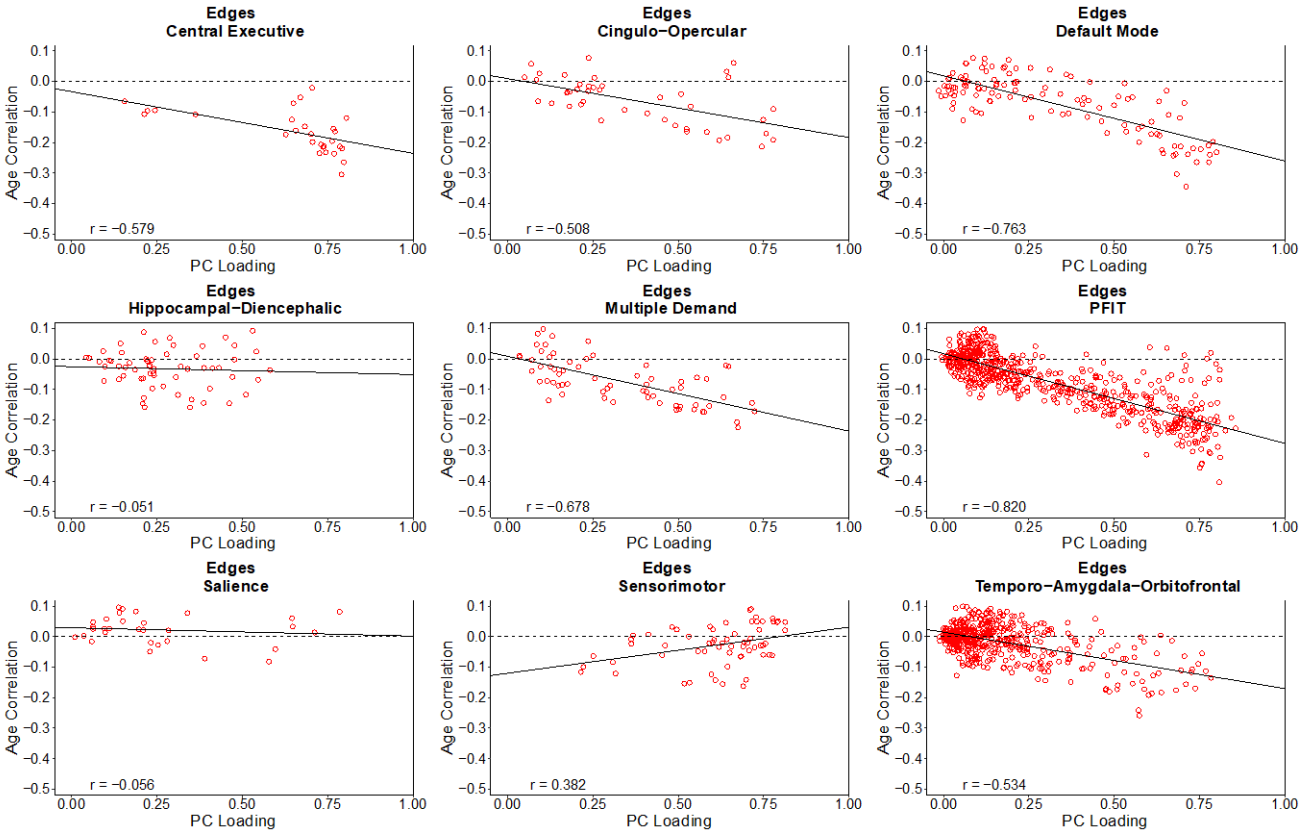

Figure S5. **Scatterplots of edge-age correlations and PC loadings in NOIs.** Correlations between edge-age correlations and loadings on the first principal component within each NOI. Dashed line represents $r = 0$. Solid line represents the regression line for age correlation on principal component loadings. Principal component loadings were standardized before analysis.

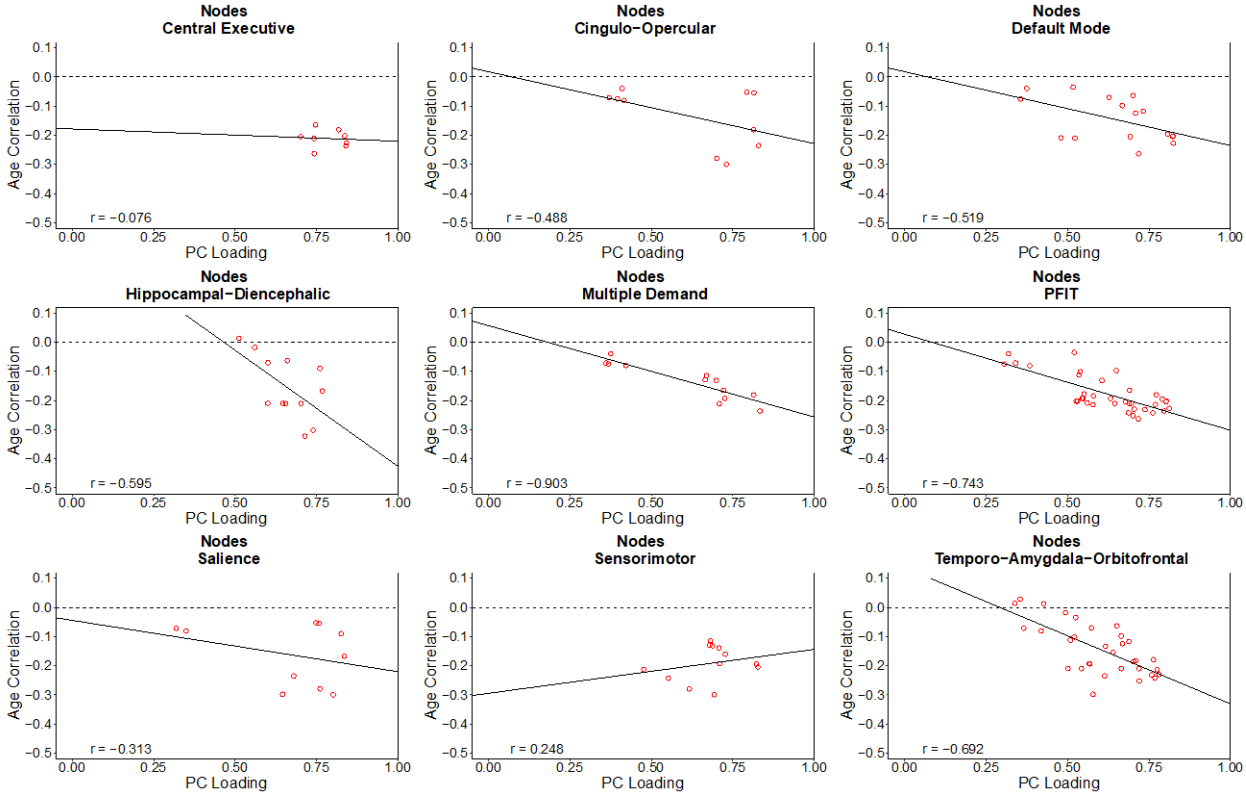

Figure S6. **Scatterplots of node-age correlations and PC loadings in NOIs**. Correlations between node-age correlations and loadings on the first principal component within each NOI. Dashed line represents $r = 0$. Solid line represents the regression line for age correlation on principal component loadings. Principal component loadings were standardized before analysis.

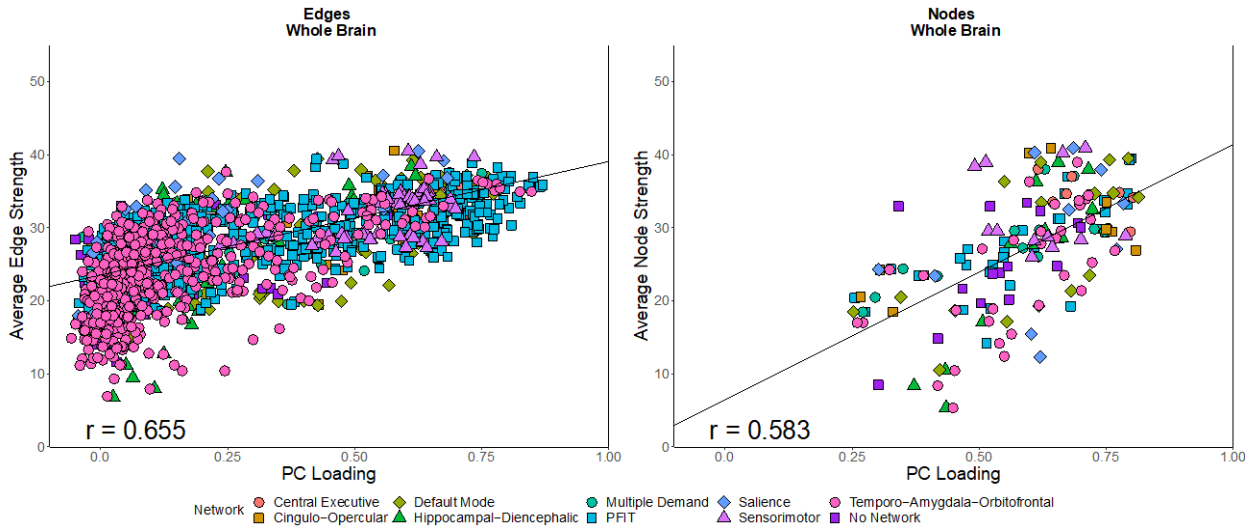

Figure S7. **Scatterplots of whole-brain topological centrality and PC loadings.** Scatterplots displaying the association between weighted topological centrality (*i.e.,* each connectome element's average strength) and representativeness of variation in connectome integrity (*i.e.,* each element's loading on the first principal component). Plots are broken down by element type (*i.e.,* edges and nodes). Each point represents a unique element of the connectome (N=3,567 non-zero edges; 85 nodes). Points are categorized by the network the element belongs to. Line represents the regression line for average strength on principal component loadings.

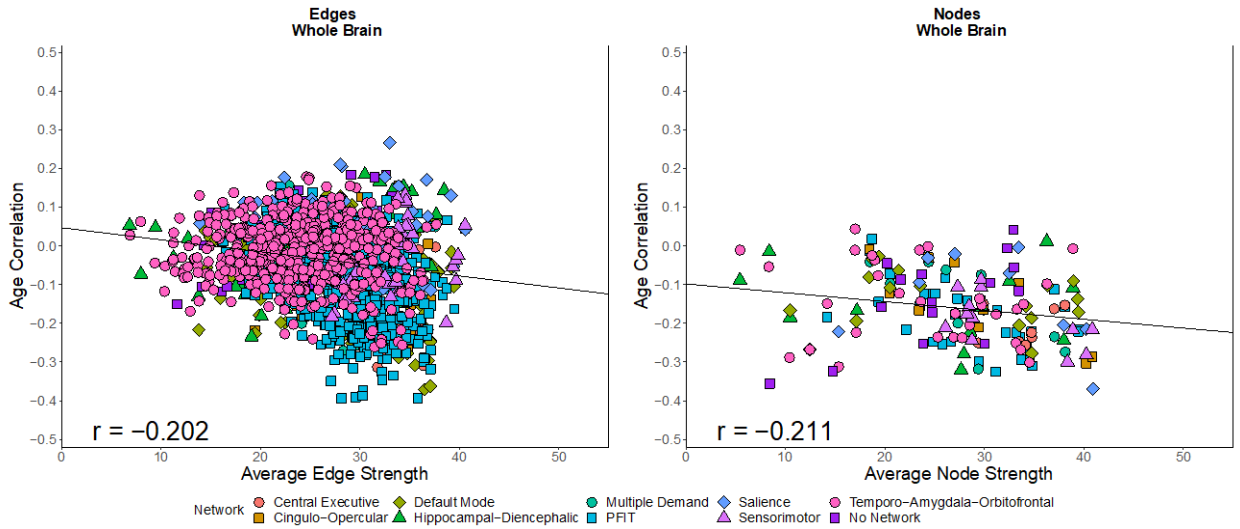

Figure S8. **Scatterplots of whole-brain topological centrality and age correlations**. Scatterplots displaying the association between each connectome element's correlation with age and each element's weighted topological centrality (*i.e.,* each connectome element's average strength). Plots are broken down by element type (*i.e.,* edges and nodes). Each point represents a unique element of the connectome (N=3,567 non-zero edges; 85 nodes). Points are categorized by the network the element belongs to. Line represents the regression line for each element's age correlations on average strength.

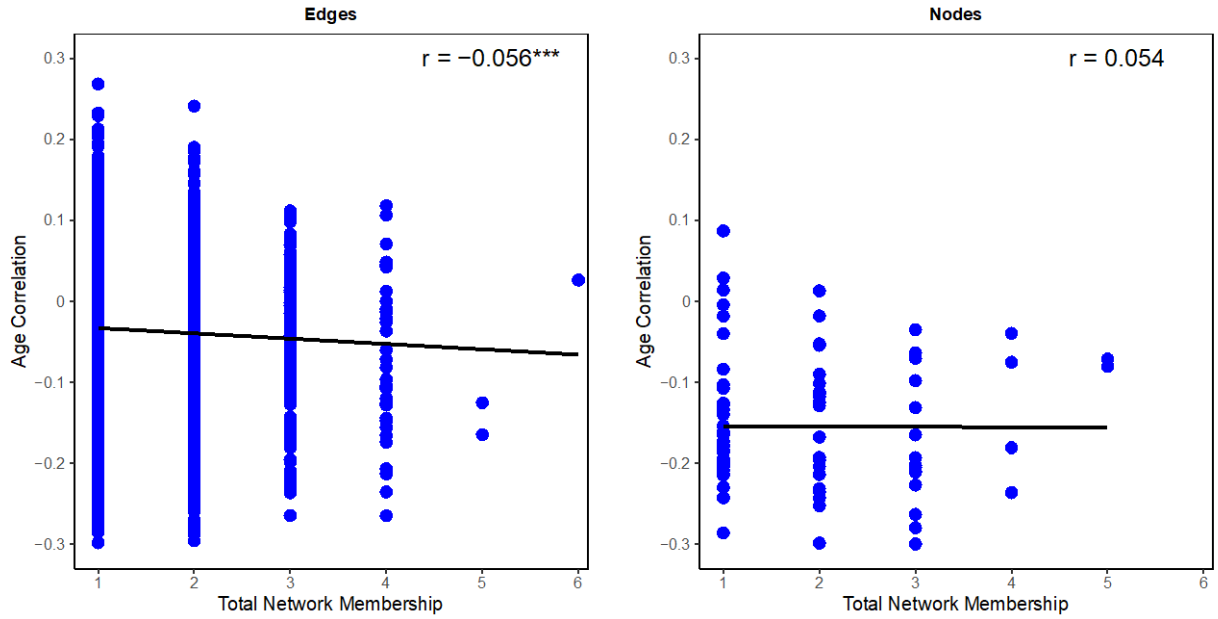

Figure S9. **Scatterplot of network membership by age correlation.** Scatterplots reflecting the total number of NOIs that an element belongs to by each element's correlation with age. Nodes belonged to between 1 and 5 networks with a median of 2 networks. Edges belonged to between 1 and 6 networks with a median of 1 network.

*** $p < 0.001$

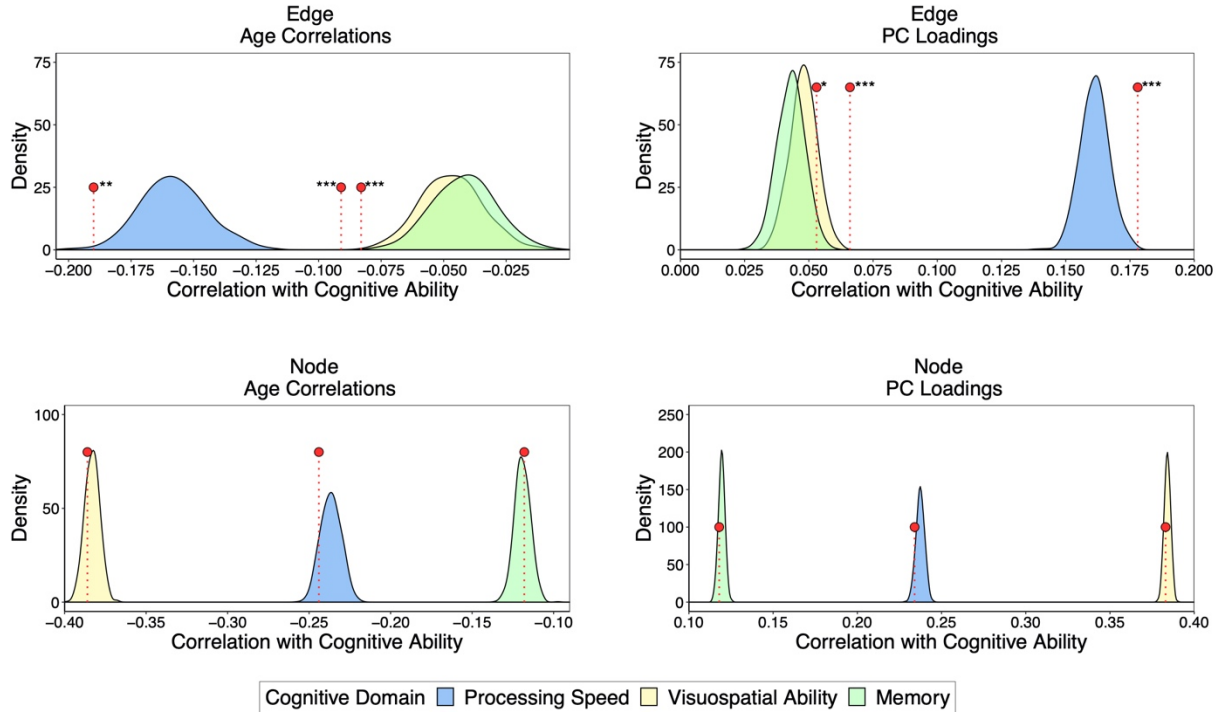

Figure S10. **Empirical distributions of associations between permuted composite scores and cognitive function.** Empirical distributions of associations between permuted weighted composite scores (k = 1,000) and domains of cognitive function. Permuted composite scores were created from both age correlations and PC loadings weights in both edges and nodes. Red data points represent observed associations between weighted composite scores and domains of cognitive function (see Fig. 4, Fig. S11, and Table S9 for reference).

* empirical $p < 0.05$; ** empirical $p < 0.01$; *** empirical $p < 0.001$

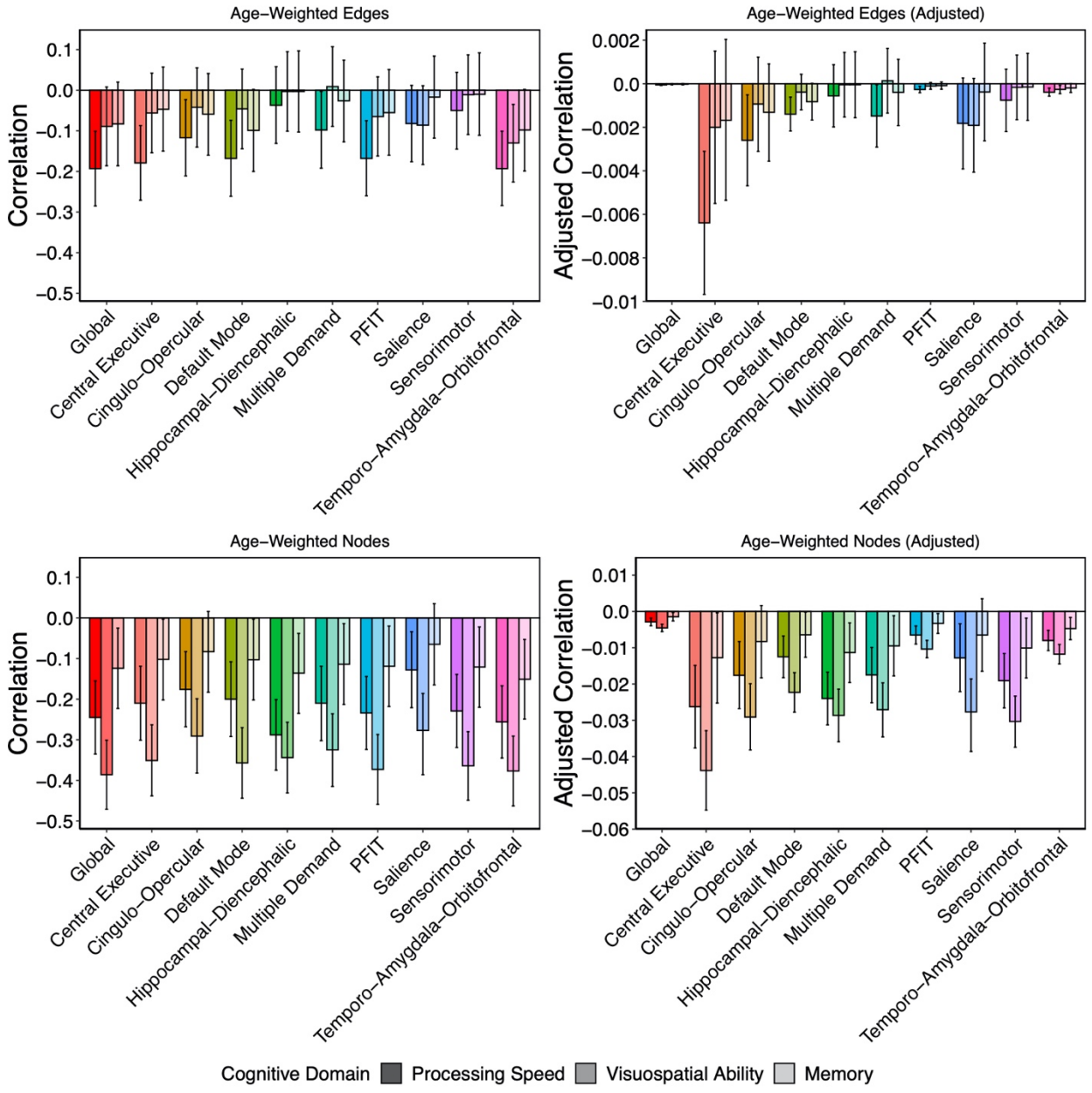

Figure S11. **Associations between age-weighted composite scores and cognitive function.** Raw and adjusted associations between weighted linear composite scores reflecting age-susceptibility and cognitive function in LBC1936. Scores were created across the whole brain and all NOIs by summing the LBC1936 data weighted by each element's age correlation discovered in UK Biobank. Plots are broken down by element type (*i.e.*, edges or nodes) and reflect correlations between composite scores from each NOI and the cognitive domains of processing speed, visuospatial ability, and memory.

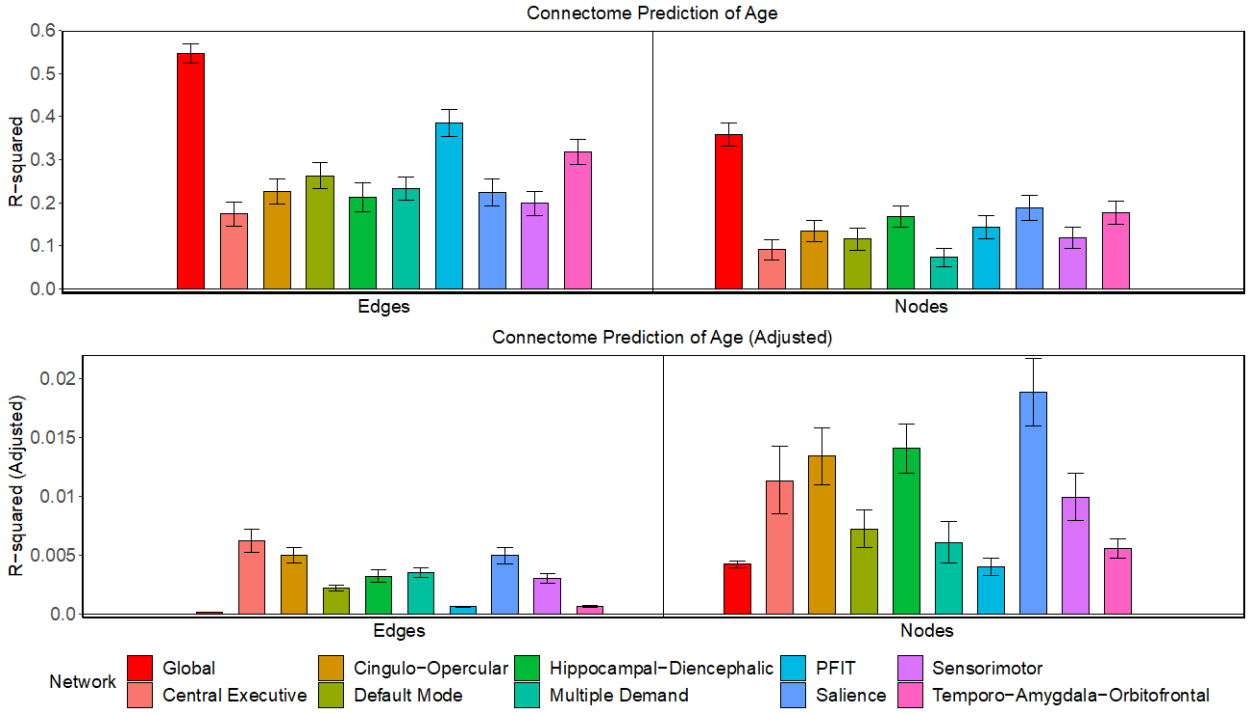

Figure S12. **LASSO-prediction of age in UKB.** LASSO-prediction of age in a UK Biobank hold-out sample from brain network-specific data trained in UK Biobank. Predictions are broken down by connectome elements (*i.e.*, edges or nodes). Prediction of age is represented as both the raw and adjusted R^2 value, with error bars representing bootstrapped 95% confidence intervals based on the 100 iterations of R^2 calculation. A full description of these findings can be found in the Supplementary Results.

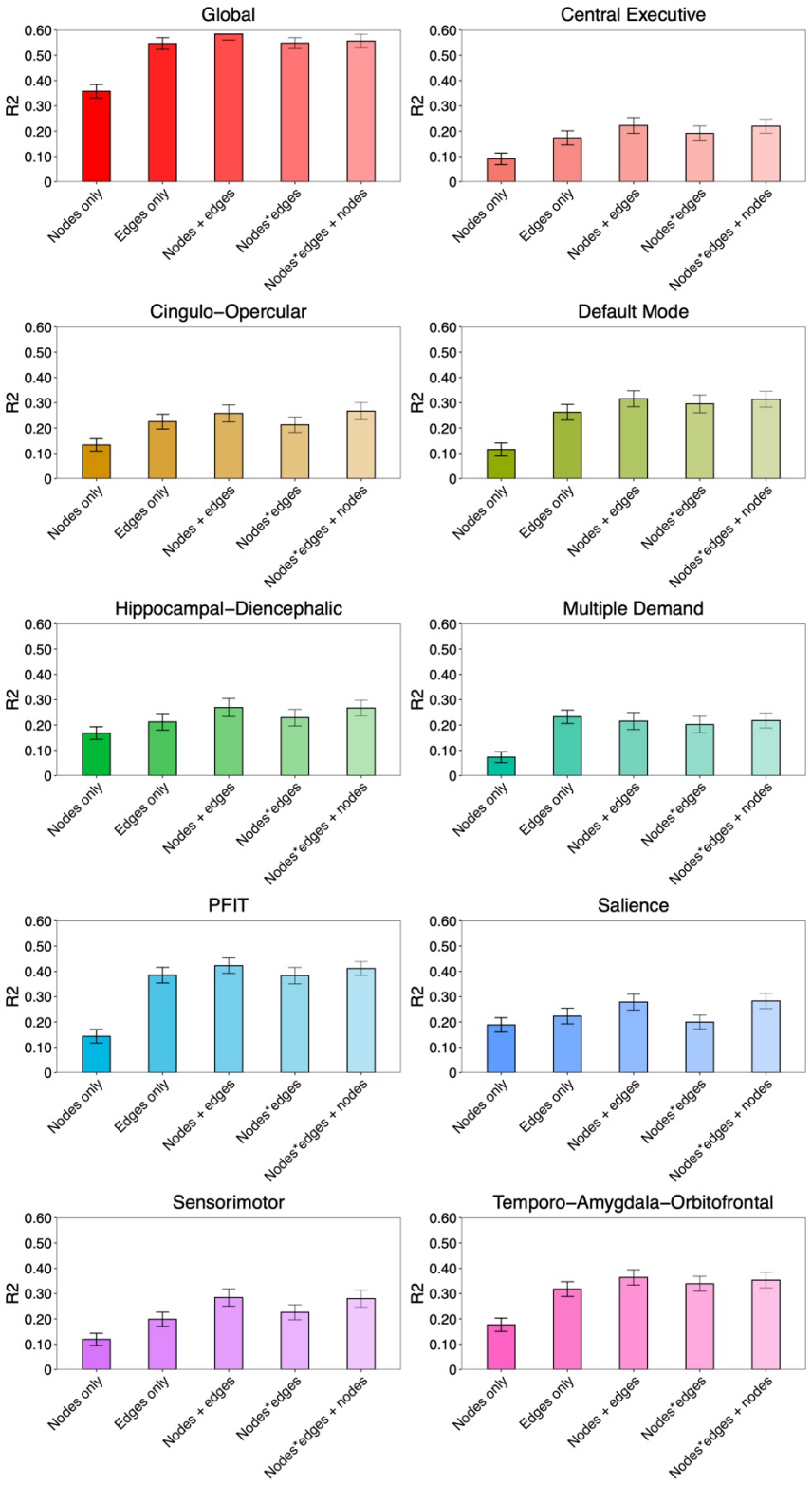

Figure S13. **LASSO-prediction of age in UKB using novel weighting schemes.** LASSO-prediction of age in each NOI broken down by weighting scheme (nodes alone, edges alone, nodes + edges, nodes*edges, nodes*edges + nodes). A full description of each weighting scheme can be found in the Supplementary Method.

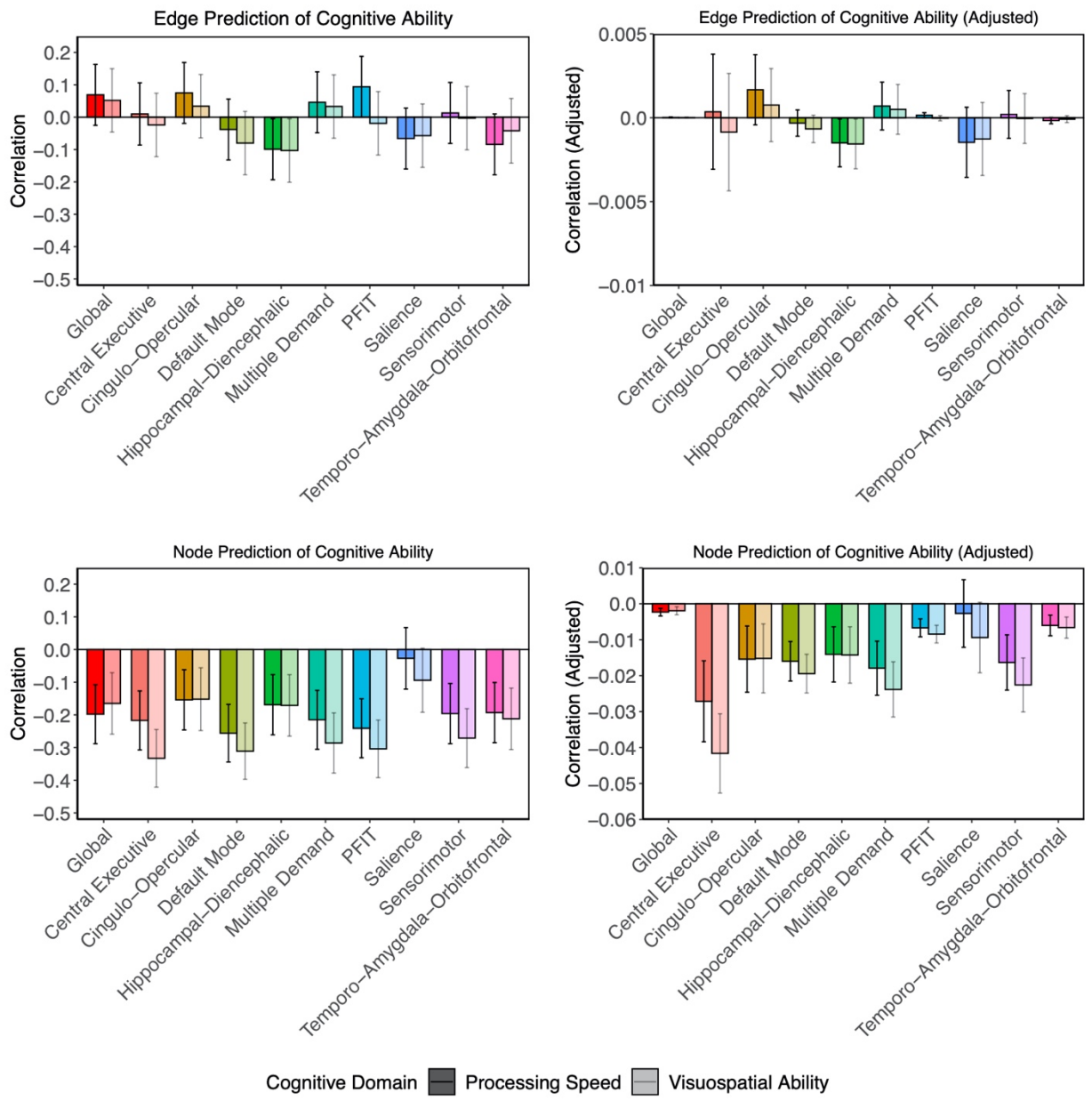

Figure S14. **LASSO-prediction of cognitive function in LBC1936.** LASSO-prediction of cognitive function (processing speed and visuospatial ability) in LBC1936 from brain network-specific age data trained in UK Biobank. Predictions are broken down by connectome elements (*i.e.*, edges or nodes). Prediction of cognitive function is represented as both the raw and adjusted correlation between LASSO-retained element-age coefficients from each NOI and latent factors of processing speed and visuospatial ability, with error bars representing 95% confidence intervals. A full description of these results can be found in the Supplementary Results.

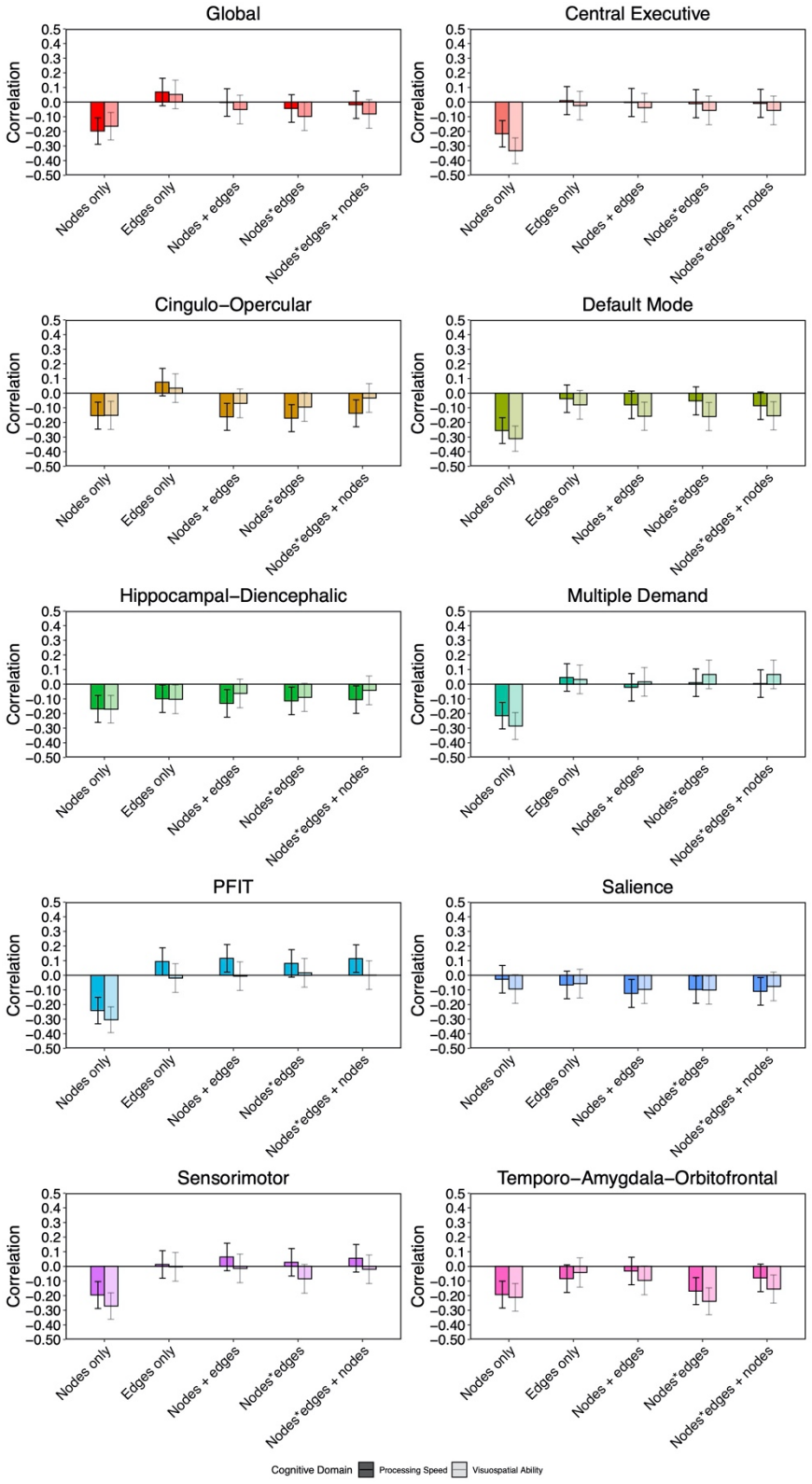

Figure S15. **LASSO-prediction of cognitive function in LBC1936 using novel weighting schemes.** LASSO-prediction of cognitive function in each network-of-interest broken down by weighting scheme (nodes alone, edges alone, nodes + edges, nodes*edges, nodes*edges + nodes). A full description of each weighting scheme can be found in the Supplementary Method.

4. Supplementary Tables

Table S1. **Assignments of each brain region to each of the nine NOIs.** Brain regions were parceled per the Desikan-Killiany atlas[10].

Node	*Central Executive*	*Cingulo-Opercular*	*Default Mode*	*Hippocampal-Diencephalic*	*Multiple Demand*	*PFIT*	*Salience*	*Sensori-motor*	*Temporo-Amygdala-Orbitofrontal*	*No Network*
Left-thalamus	0	1	0	0	0	0	1	1	0	0
Left-caudate	0	0	0	0	0	0	0	0	0	1
Left-putamen	0	0	0	0	0	0	0	1	0	0
Left-pallidum	0	0	0	0	0	0	0	0	0	1
Brain stem	0	0	0	0	0	0	0	0	0	1
Left-hippocampus	0	0	0	1	0	0	0	0	0	0
Left-amygdala	0	0	0	0	0	0	1	0	1	0
Left-accumbens area	0	0	0	0	0	0	0	0	0	1
Left-ventral diencephalon	0	0	0	1	0	0	1	0	0	0
Right-thalamus	0	1	0	0	0	0	1	1	0	0
Right-caudate	0	0	0	0	0	0	0	0	0	1
Right-putamen	0	0	0	0	0	0	0	1	0	0
Right-pallidum	0	0	0	0	0	0	0	0	0	1
Right-hippocampus	0	0	0	1	0	0	0	0	0	0
Right-amygdala	0	0	0	0	0	0	1	0	1	0
Right-accumbens area	0	0	0	0	0	0	0	0	0	1
Right-ventral diencephalon	0	0	0	1	0	0	1	0	0	0
Left-superior temporal sulcus	0	0	0	0	0	1	0	0	1	0
Left-caudal anterior cingulate	0	1	0	0	1	1	1	0	1	0
Left-caudal middle frontal	0	0	0	0	1	1	0	1	0	0
Left-cuneus	0	0	0	0	0	0	0	0	0	1
Left-entorhinal	0	0	0	1	0	0	0	0	1	0
Left-fusiform	0	0	0	1	0	1	0	0	1	0
Left-inferior parietal	1	0	1	0	0	1	0	0	0	0
Left-inferior temporal	0	0	0	0	0	0	0	0	1	0
Left-isthmus cingulate	0	0	1	1	0	0	0	0	1	0
Left-lateral occipital	0	0	0	0	0	1	0	0	0	0
Left-lateral orbitofrontal	0	0	0	0	0	0	0	0	1	0
Left-lingual	0	0	0	0	0	0	0	0	0	1
Left-medial orbitofrontal	0	0	1	0	0	0	0	0	1	0
Left-middle temporal	0	0	0	0	0	1	0	0	1	0
Left-parahippocampal	0	0	1	1	0	0	0	0	1	0

Node	*Central Executive*	*Cingulo-Opercular*	*Default Mode*	*Hippocampal-Diencephalic*	*Multiple Demand*	*PFIT*	*Salience*	*Sensori-motor*	*Temporo-Amygdala-Orbitofrontal*	*No Network*
Left-paracentral	0	0	0	0	1	0	0	1	0	0
Left-pars opercularis	0	0	0	0	0	1	0	0	0	0
Left-pars orbitalis	0	0	0	0	0	1	0	0	0	0
Left-pars triangularis	0	0	0	0	0	1	0	0	0	0
Left-pericalcarine	0	0	0	0	0	0	0	0	0	1
Left-postcentral	0	0	0	0	0	0	0	1	0	0
Left-posterior cingulate	0	0	0	0	0	0	0	0	1	0
Left-precentral	0	0	0	0	0	0	0	1	0	0
Left-precuneus	0	0	1	0	0	1	0	0	0	0
Left-rostral anterior cingulate	0	0	1	0	0	1	0	0	1	0
Left-rostral middle frontal	1	1	0	0	1	1	0	0	0	0
Left-superior frontal	1	0	1	0	0	1	0	0	0	0
Left-superior parietal	1	0	0	0	1	1	0	0	0	0
Left-superior temporal	0	0	0	0	0	1	0	0	1	0
Left-supramarginal	0	0	0	0	0	0	0	0	0	1
Left-frontal pole	0	1	1	0	1	1	0	0	0	0
Left-temporal pole	0	0	0	0	0	0	0	0	1	0
Left-transverse temporal	0	0	0	0	0	1	0	0	1	0
Left-insula	0	1	0	0	0	0	1	0	0	0
Right-superior temporal sulcus	0	0	0	0	0	1	0	0	1	0
Right-caudal anterior cingulate	0	1	0	0	1	1	1	0	1	0
Right-caudal middle frontal	0	0	0	0	1	1	0	1	0	0
Right-cuneus	0	0	0	0	0	0	0	0	0	1
Right-entorhinal	0	0	0	1	0	0	0	0	1	0
Right-fusiform	0	0	0	1	0	1	0	0	1	0
Right-inferior parietal	1	0	1	0	0	1	0	0	0	0
Right-inferior temporal	0	0	0	0	0	0	0	0	1	0
Right-isthmus cingulate	0	0	1	1	0	0	0	0	1	0
Right-lateral occipital	0	0	0	0	0	1	0	0	0	0
Right-lateral orbitofrontal	0	0	0	0	0	0	0	0	1	0
Right-lingual	0	0	0	0	0	0	0	0	0	1
Right-medial orbitofrontal	0	0	1	0	0	0	0	0	1	0
Right-middle temporal	0	0	0	0	0	1	0	0	1	0
Right-parahippocampal	0	0	1	1	0	0	0	0	1	0
Right-paracentral	0	0	0	0	1	0	0	1	0	0
Right-pars opercularis	0	0	0	0	0	1	0	0	0	0

Node	*Central Executive*	*Cingulo-Opercular*	*Default Mode*	*Hippocampal-Diencephalic*	*Multiple Demand*	*PFIT*	*Salience*	*Sensori-motor*	*Temporo-Amygdala-Orbitofrontal*	*No Network*
Right-pars orbitalis	0	0	0	0	0	1	0	0	0	0
Right-pars triangularis	0	0	0	0	0	1	0	0	0	0
Right-pericalcarine	0	0	0	0	0	0	0	0	0	1
Right-postcentral	0	0	0	0	0	0	0	1	0	0
Right-posterior cingulate	0	0	0	0	0	0	0	0	1	0
Right-precentral	0	0	0	0	0	0	0	1	0	0
Right-precuneus	0	0	1	0	0	1	0	0	0	0
Right-rostral anterior cingulate	0	0	1	0	0	1	0	0	1	0
Right-rostral middle frontal	1	1	0	0	1	1	0	0	0	0
Right-superior frontal	1	0	1	0	0	1	0	0	0	0
Right-superior parietal	1	0	0	0	1	1	0	0	0	0
Right-superior temporal	0	0	0	0	0	1	0	0	1	0
Right-supramarginal	0	0	0	0	0	0	0	0	0	1
Right-frontal pole	0	1	1	0	1	1	0	0	0	0
Right-temporal pole	0	0	0	0	0	0	0	0	1	0
Right-transverse temporal	0	0	0	0	0	1	0	0	1	0
Right-insula	0	1	0	0	0	0	1	0	0	0

Table S2. **Comparison of NOIs to Yeo et al.[23] networks.**

Presently-examined NOI	Yeo et al. (2011)
Central Executive	Frontoparietal (Orange)[a] + Default (Red)[b]
Cingulo-Opercular	Frontoparietal (Orange)[a] + Ventral Attention (Violet)[c]
Default Mode	Default (Red)
Hippocampal-Diencephalic	Default (Red)[d]
Multiple Demand	Frontoparietal (Orange)
PFIT	Default (Red) + Frontoparietal (Orange) + Dorsal Attention (Green)
Salience	Frontoparietal (Orange)[e] + Ventral Attention (Violet)[c]
Sensorimotor	Somatomotor (Blue)
Temporo-Amygdala-Orbitofrontal	Limbic (Cream)[f]

Note. Colors in parentheses refer to schematic designation in Fig. 11 of Yeo et al. (2011). Only a cortical comparison is possible as no subcortical involvement was considered in Yeo et al. (2011). [a] = minus cingulate; [b] = minus superior temporal; [c] = insular aspect only; [d] = posterior aspects only; [e] = cingulate aspect only; [f] = plus cingulate and temporal.

Table S3. **Unique elements within each NOI.**

Network	Total Nodes	Unique Nodes	Total Edges	Unique Edges
Central Executive	8	0	28	0
Cingulo-Opercular	10	0	45	16
Default Mode	16	0	120	48
Hippocampal-Diencephalic	12	2	66	37
Multiple Demand	12	0	66	16
PFIT	36	8	630	436
Salience	10	0	45	24
Sensorimotor	12	6	66	59
Temporo-Amygdala-Orbitofrontal	32	8	496	352

Note. Within each network, the total number of edges is equal to N*((N-1)/2), where N equals the number of nodes. This same mathematical principal does not apply to the estimation of unique elements within a network. Two nodes may be present across several networks, but may only be jointly present within a single subnetwork, thus returning a unique edge for that subnetwork, but not unique nodes. 24 out of 85 nodes (28.2%) are unique to specific networks. 2210 edges are not a part of any network because they connect two nodes that are not jointly present within a single subnetwork. Of the edges that occur within networks, 988 out 1360 (72.6%) are unique.

Table S4. **Model fit and descriptive statistics for cognitive tests in LBC1936.** Descriptive statistics, intercorrelations, and factor parameters for the cognitive tasks in LBC1936.

Cognitive Task	*Mean*	*SD*	*Range*	*Factor Loading*	*Intercorrelations*										
Visuospatial Reasoning CFI = 0.913; TLI = 0.739; RMSEA = 0.180; SRMR = 0.049					**MR**	**BD**	**SSF**	**SSB**	**DSS**	**SS**	**CRT**	**IT**	**LM**	**VPA**	**DB**
Matrix Reasoning (MR)	13.4	4.9	3 - 25	0.663	1										
Block Design (BD)	34.3	10.1	10 - 65	0.764	.541	1									
Spatial Span (Forward) (SSF)	7.6	1.6	3 - 12	0.462	.272	.308	1								
Spatial Span (Backward) (SSB)	7.1	1.6	1 - 11	0.543	.306	.398	.413	1							
Processing Speed CFI = 1.0; TLI = 0.999; RMSEA = 0.009; SRMR = 0.011															
Digit-Symbol Substitution (DSS)	56.6	11.6	26 - 94	0.821	.333	.438	.272	.271	1						
Symbol Search (SS)	25.8	6.0	4 - 43	0.748	.332	.467	.288	.325	.620	1					
Choice Reaction Time* (CRT)	-64.4	8.5	-108 - -45.9	0.645	.184	.279	.276	.252	.528	.473	1				
Inspection Time (IT)	111.4	10.9	67 - 134	0.462	.218	.259	.218	.258	.366	.341	.335	1			
Memory CFI = 1.0; TLI = 1.0; RMSEA = 0.0; SRMR = 0.0															
Logical Memory (LM)	74.7	17.9	17 - 116	0.784	.340	.259	.160	.155	.339	.279	.223	.184	1		
Verbal Paired Associates (VPA)	27.5	9.5	0 - 40	0.684	.333	.284	.157	.161	.335	.259	.216	.231	.530	1	
Digits Backwards (DB)	7.91	2.3	2 - 14	0.414	.343	.311	.268	.286	.354	.316	.222	.175	.325	.282	1

Note. Between 1 and 13 participants had missing data across all tests. CRT scores were multiplied by -100 such that higher scores are associated with faster performance. The model for Memory was fully saturated and thus returned perfect model fit. The Logical Memory and Verbal Paired Associates measures were created by summing the number of items that each participant recalled correctly across both the immediate- and delayed-recall versions of the task.

Table S5. **Hartigans' dip-test for bimodality.**

Network	**Estimate** *Edges - Age Correlations*	**Estimate** *Edges - PC Loadings*	**Estimate** *Nodes - Age Correlations*	**Estimate** *Nodes - PC Loadings*
Global	0.003 (0.998)	0.006 (0.528)	0.026 (0.969)	0.032 (0.793)
Central Executive	0.001 (1.000)	0.055 (0.762)	0.029 (0.899)	0.176 (0.008)
Cingulo-Opercular	0.000 (1.000)	0.057 (0.319)	0.017 (1.000)	0.173 (0.003)
Default Mode	0.001 (1.000)	0.031 (0.616)	0.030 (0.886)	0.101 (0.160)
Hippocampal-Diencephalic	0.001 (1.000)	0.033 (0.906)	0.023 (0.992)	0.082 (0.713)
Multiple Demand	0.001 (1.000)	0.048 (0.300)	0.016 (1.000)	0.133 (0.041)
PFIT	0.002 (1.000)	0.028 (0.001)*	0.088 (<0.0005)*	0.068 (0.201)
Salience	0.001 (1.000)	0.040 (0.883)	0.017 (1.000)	0.091 (0.685)
Sensorimotor	0.001 (1.000)	0.029 (0.979)	0.028 (0.929)	0.079 (0.7682)
Temporo-Amygdala-Orbitofrontal	0.001 (1.000)	0.010 (0.994)	0.041 (0.385)	0.050 (0.815)

Note. P-values are in parentheses. Hartigans' dip-test is a significance test that measures the deviation of a distribution from unimodality[24]. Significance threshold was Bonferroni corrected for 20 significance tests, rather than for the complete set of 40 significance tests that were conducted, given the substantial overlap between the age correlations and PC loadings. * denotes estimates that survived Bonferroni correction.

Table S6. **Average age-element associations within NOIs.**

Network	Average Age-Edge Correlation	Average Age-Node Correlation
Global	-0.037 (0.086)	-0.160 (0.086)
Central Executive	-0.163 (0.070)	-0.211 (0.031)
Cingulo-Opercular	-0.055 (0.083)	-0.137 (0.102)
Default Mode	-0.067 (0.094)	-0.146 (0.076)
Hippocampal-Diencephalic	-0.018 (0.074)	-0.155 (0.108)
Multiple Demand	-0.071 (0.074)	-0.135 (0.062)
PFIT	-0.074 (0.093)	-0.179 (0.062)
Salience	0.060 (0.072)	-0.163 (0.106)
Sensorimotor	-0.021 (0.069)	-0.192 (0.060)
Temporo-Amygdala-Orbitofrontal	-0.013 (0.060)	-0.144 (0.087)

Note. Standard deviations are in parentheses.

Table S7. **Interquartile range and Eigen decomposition for PC-weighted composite scores.** Interquartile range and percentage of variation explained by first principal component for correlations between PC-weighted linear composites across the nine NOIs (see Fig. S3). Ranges include composites created for the whole brain networks.

Element	***0%***	***25%***	***50%***	***75%***	***100%***	***% of variation explained by first PC***
PC-based composites						
Edges	0.042	0.396	0.567	0.751	0.956	62.2
Nodes	0.659	0.749	0.830	0.892	0.985	84.7

Table S8. **Correlations between edge- and node-based composite scores within NOIs.**

Network	***r*** **PC-weighted Edges & Nodes**
Global	.105 (.015)
Central Executive	.081 (.062)
Cingulo-Opercular	.138 (.001)
Default Mode	.016 (.712)
Hippocampal-Diencephalic	.048 (.276)
Multiple Demand	.081 (.062)
PFIT	.102 (.019)
Salience	.104 (.017)
Sensorimotor	.121 (.005)
Temporo-Amygdala-Orbitofrontal	.017 (.691)

Note. P-values are in parentheses.

Table S9. **Interquartile range for associations between permuted composite scores and cognitive function.** Lower and upper 2.5% boundaries of permuted distributions for associations between permuted composite scores and cognitive function (see Fig. S10). 95% IQR represents the difference between the upper and lower bounds of each distribution.

Visuospatial Ability			
Element	*Lower 2.5%*	*Upper 2.5%*	*95% IQR*
Age-based composites			
Edges	-0.071	-0.023	0.048
Nodes	-0.392	-0.374	0.018
PC-based composites			
Edges	0.037	0.058	0.021
Nodes	0.381	0.388	0.007

Processing Speed			
Element	*Lower 2.5%*	*Upper 2.5%*	*95% IQR*
Age-based composites			
Edges	-0.183	-0.131	0.052
Nodes	-0.248	-0.225	0.023
PC-based composites			
Edges	0.150	0.173	0.023
Nodes	0.232	0.242	0.010

Memory			
Element	*Lower 2.5%*	*Upper 2.5%*	*95% IQR*
Age-based composites			
Edges	-0.066	-0.018	0.048
Nodes	-0.129	-0.110	0.019
PC-based composites			
Edges	0.033	0.053	0.020
Nodes	0.116	0.123	0.008

Table S10. **UKB-derived age- and PC-weights for connectome elements.**

Note: Due to the size of this table, it is only accessible as an Excel file.

5. Supplementary References

1. Sudlow, C. *et al.* UK biobank: an open access resource for identifying the causes of a wide range of complex diseases of middle and old age. *PLoS Med.* **12**, e1001779 (2015).
2. Gong, G. *et al.* Age- and Gender-Related Differences in the Cortical Anatomical Network. *J. Neurosci.* **29**, 15684–15693 (2009).
3. Ritchie, S. J. *et al.* Sex Differences in the Adult Human Brain: Evidence from 5216 UK Biobank Participants. *Cereb. Cortex* **28**, 2959–2975 (2018).
4. *The Intelligence of Scottish Children*. (University of London Press, 1933).
5. Deary, I. J., Gow, A. J., Pattie, A. & Starr, J. M. Cohort profile: the Lothian Birth Cohorts of 1921 and 1936. *Int. J. Epidemiol.* **41**, 1576–1584 (2012).
6. Taylor, A. M., Pattie, A. & Deary, I. J. Cohort Profile Update: The Lothian Birth Cohorts of 1921 and 1936. *Int. J. Epidemiol.* **47**, 1042–1042r (2018).
7. Miller, K. L. *et al.* Multimodal population brain imaging in the UK Biobank prospective epidemiological study. *Nat. Neurosci.* **19**, 1523–1536 (2016).
8. Alfaro-Almagro, F. *et al.* Image processing and Quality Control for the first 10,000 brain imaging datasets from UK Biobank. *NeuroImage* **166**, 400–424 (2018).
9. Fischl, B. & Dale, A. M. Measuring the thickness of the human cerebral cortex from magnetic resonance images. *Proc. Natl. Acad. Sci. U. S. A.* **97**, 11050–11055 (2000).
10. Desikan, R. S. *et al.* An automated labeling system for subdividing the human cerebral cortex on MRI scans into gyral based regions of interest. *NeuroImage* **31**, 968–980 (2006).
11. Fischl, B. *et al.* Whole brain segmentation: automated labeling of neuroanatomical structures in the human brain. *Neuron* **33**, 341–355 (2002).
12. Wardlaw, J. M. *et al.* Brain aging, cognition in youth and old age and vascular disease in the Lothian Birth Cohort 1936: rationale, design and methodology of the imaging protocol. *Int. J. Stroke Off. J. Int. Stroke Soc.* **6**, 547–559 (2011).
13. Behrens, T. E. J. *et al.* Non-invasive mapping of connections between human thalamus and cortex using diffusion imaging. *Nat. Neurosci.* **6**, 750–757 (2003).
14. R Core Team. *R: A language and environment for statistical computing*. (R Foundation for Statistical Computing, 2018).
15. Wickham, H. *Ggplot2: elegant graphics for data analysis*. (Springer, 2009).
16. Xia, M., Wang, J. & He, Y. BrainNet Viewer: A Network Visualization Tool for Human Brain Connectomics. *PLoS ONE* **8**, e68910 (2013).
17. Rosseel, Y. **lavaan** : An *R* Package for Structural Equation Modeling. *J. Stat. Softw.* **48**, (2012).

18. Friedman, J., Hastie, T. & Tibshirani, R. Regularization Paths for Generalized Linear Models via Coordinate Descent. *J. Stat. Softw.* **33**, 1–22 (2010).

19. Kuhn et al. *caret: Classification and Regression Training*. (2019).

20. Gabor Csardi and Tamas Nepusz. *The igraph software package for complex network research*. (2006).

21. Buchanan, C. R. *et al.* The effect of network thresholding and weighting on structural brain networks in the UK Biobank. *NeuroImage* **211**, 116443 (2020).

22. Poldrack, R. A., Huckins, G. & Varoquaux, G. Establishment of Best Practices for Evidence for Prediction: A Review. *JAMA Psychiatry* (2019) doi:10.1001/jamapsychiatry.2019.3671.

23. Yeo, B. T. *et al.* The organization of the human cerebral cortex estimated by intrinsic functional connectivity. *J. Neurophysiol.* **106**, 1125–1165 (2011).

24. Hartigan, J. A. & Hartigan, P.M. The dip test of unimodality. *Ann. Stat.* **13**, 70–84 (1985).